



1 Why Did Ozone Concentrations Increase During Shanghai's Static 2 Management? A Statistical and Radical Chemistry Perspective

3 Jian Zhu¹, Shanshan Wang^{1,2}, Chuanqi Gu¹, Zhiwen Jiang¹, Sanbao Zhang¹, Ruibin Xue¹, Yuhao Yan¹, Bin
4 Zhou^{1,2,3}

5 ¹Shanghai Key Laboratory of Atmospheric Particle Pollution and Prevention (LAP³), Department of Environmental Science and
6 Engineering, Fudan University, Shanghai, 200433, China.

7 ²Institute of Eco-Chongming (IEC), Shanghai, 202162, China.

8 ³Institute of Atmospheric Sciences, Fudan University, Shanghai, 200433, China.

9 Correspondence to: Bin Zhou (binzhou@fudan.edu.cn) and Shanshan Wang (shanshanwang@fudan.edu.cn)

10 Abstract

11 During the period of April and May 2022, Shanghai implemented city-wide static management measures to control the spread of
12 the Omicron variant. Compared to the lockdown in early 2020, the static management in 2022 occurred during the high-ozone
13 season and lasted for a longer duration. It can be considered as a “large-scale field experiment” to study the response of ambient
14 ozone levels to emission reductions. During this period, we conducted comprehensive observations at Fudan University
15 Jiangwan Campus in the northeast corner of Shanghai. Similar experiments were also conducted during the same period in 2020
16 and 2021. Despite the significant reduction of approximately 30% in VOCs and around 50% in NO₂ due to static management in
17 2022, the average ozone level increased by nearly 23%. This suggests that the reduction in ozone precursors and other pollutants
18 did not lead to a corresponding decrease in ozone concentrations as expected. Cluster analysis of diurnal patterns of ozone
19 concentration revealed four distinct types of diurnal ozone variations. Cluster 3 and Cluster 4, with high ozone levels,
20 experienced significant increases in their share during static management, ultimately leading to an overall increase in average
21 ozone levels in 2022. According to the Observation-Based Model (OBM) simulation analysis, the average peak concentrations of
22 OH, HO₂, and RO₂ in 2022 were estimated to be 5.3×10^6 , 4.9×10^8 , and 2.6×10^8 molecules cm⁻³, respectively, representing an
23 increase of over 30% compared to the levels in 2020 and 2021. Although HONO photolysis was the main contributor to the
24 primary source of RO_x radicals, the radical cycling process remained dominant for the overall production of RO_x radicals. Due
25 to a significant decrease in NO₂ concentration relative to VOCs, the average VOCs/NO₂ ratio increased from 1.6 in 2020 to 3.0
26 in 2022, which is also reflected in the radical cycling. The ratio of OH radical propagation (OH+VOCs) to termination (OH+NO₂)
27 was 2.10, higher than 1.03 in 2020 and 1.60 in 2021, indicating that the different reduction proportions of precursors led to a
28 higher VOCs/NO₂ ratio, strengthening the radical cycling. The differential reduction in precursor VOCs and NO₂ levels due to
29 static management is the underlying cause for the increase in ozone concentration in Shanghai.

30 1 Introduction

31 To curb the spread of Omicron variant in Shanghai, China, the local government decided to implement city-wide static
32 management in early April 2022. The strict two-month lockdown severely impacted the economic activities and human life of
33 this mega city. According to official statistics, in April and May 2022, Shanghai experienced a year-on-year decrease of 42% in
34 its total industrial output value. Moreover, the total volume of transported goods decreased by 30% year-on-year, with road
35 transport witnessing a significant drop of 64%. Additionally, the port cargo throughput decreased by 31% year-on-year. The
36 direct effect of such lockdown policies on air quality is a significant reduction in anthropogenic emissions, which can be



37 considered as an ideal experiment on emissions control in a mega-city to explore the reduction potential and response of air
38 quality . It makes sense to take advantage of this rare yet regrettable window to study the causes and management of air pollution,
39 especially in those countries like China that face air pollution complex.

40 Prior to this, China had implemented a series of nationwide lockdown measures against the occurrence and spread of the virus in
41 early 2020. This reduction in human activity is expected to significantly reduce air pollutant emissions, as confirmed by lots of
42 studies on lockdown in 2020 (Bao and Zhang, 2020; Huang et al., 2021; Li et al., 2021b; Liu et al., 2020; Tian et al., 2021; Wang
43 et al., 2021; Zhang et al., 2022b). Reports on the impact of the lockdown on air quality most commonly focus on measuring
44 nitrogen dioxide (NO₂) and fine particulate matter (PM_{2.5}) (Agarwal et al., 2020; Hua et al., 2021; Chu et al., 2021). Among
45 these pollutants, NO₂ from traffic sources has shown the most significant reduction, with traffic-related NO₂ exhibiting the
46 largest decrease (Rana et al., 2021). Due to the lockdown taking place during winter, which is a season of high particulate matter
47 pollution in China, the reports on the impact of the lockdown on air quality have focused more on the changes in particulate
48 matter. The lockdown in Shanghai in 2022 was implemented in April and May during the high-ozone (O₃) season and lasted for
49 a longer duration, providing an opportunity to study atmospheric pollution primarily caused by O₃.

50 Previous extensive research has demonstrated that the formation of O₃ in response to its precursors is highly nonlinear, rather
51 than linear, which presents a challenge in ozone control (Liu and Shi, 2021; Wang et al., 2017; Sillman, 1999). The COVID-19
52 pandemic provided a costly experiment to validate this. during the static management period in Shanghai, despite a reduction in
53 precursor emissions, the ozone levels increased compared to the previous year. The cause of this increase is attributed to an
54 imbalance in the reduction ratio of nitrogen oxides (NO_x) and volatile organic compounds (VOCs) rather than meteorological
55 conditions, according to satellite observation results (Tan and Wang, 2022; Xue et al., 2022). In this current study, aim is to
56 elucidate the reasons behind the increase in ozone levels in Shanghai through a comprehensive approach involving in-situ
57 observations, mathematical analysis, and modeling. Benefitting from our conducted routine observational campaigns, we have
58 obtained comprehensive observational data for both the static management period and corresponding historical periods. We
59 initiated our analysis by comparing pollutant levels and diurnal variations during the static management period with those from
60 historical reference periods. Subsequently, by clustering diurnal ozone profile patterns, we examined the reasons behind the
61 elevated ozone levels from a statistical perspective. Furthermore, we discuss changes in radical chemistry compared to historical
62 periods, shedding light on the increase in ozone concentrations from a photochemical process standpoint. It is worth mentioning
63 that, based on previous researchs and our analysis, meteorological conditions are not considered to be the primary cause of the
64 ozone increase during the static management period, even though we acknowledge that meteorological conditions are indeed
65 important factors influencing ozone levels. The in-depth comparison of meteorological conditions is presented in Text S1 of the
66 Supplement.

67 **2 Experimental Details and Methods**

68 **2.1 Location and Experimental Setup**

69 During the static management period in April and May of 2022, we conducted comprehensive observational experiments at
70 Fudan University's Jiangwan Campus (31.34°N, 121.51°E), located in an urban area in northeastern Shanghai, China. Similar
71 experiments were also conducted during the corresponding period in 2020 and 2021. The ambient concentrations of O₃, NO₂,
72 SO₂, HONO, and HCHO were measured using the Differential Optical Absorption Spectroscopy (DOAS) system located on the
73 rooftop of the Environmental Science Building (Zhu et al., 2020; Guo et al., 2021; Zhu et al., 2022). Based on the given optical
74 path length and integration time, the detection limits for O₃, NO₂, SO₂, HONO, and HCHO were approximately 1.3 ppbv, 0.5



75 ppbv, 0.1 ppbv, 0.1 ppbv, and 0.5 ppbv, respectively. The measurements were carried out with a time resolution of 5-6 minutes
76 and detailed fitting configurations are available in Table S1. Non-methane volatile organic compounds (NMVOCs) were
77 monitored in real-time using the TH-300B online monitoring instrument, which has been previously described in detail in
78 previous reports (Gu et al., 2022; Zhu et al., 2020). The photolysis rate of NO₂ ($j(\text{NO}_2)$) was measured using a filter radiometer
79 (Meteorologieconsult GmbH, Germany). The meteorological parameters data such as pressure (P), temperature (TEMP), relative
80 humidity (RH), wind speed (WS), wind direction (WD), and boundary layer height (BLH) are derived from the European Center
81 for Medium-Range Weather Forecasts (ECMWF) atmospheric reanalysis product ERA5 and extracted from the nest where the
82 measurement site is located. The PM_{2.5} data was obtained from the Yangpu environment monitoring station (31.53°N, 31.25°E)
83 near the measurement site.

84 2.2 Observation-Based Model (OBM)

85 The open-source zero-dimensional box model tool AtChem2 was used to simulate atmospheric chemical processes, which is
86 specifically designed for use with the Master Chemical Mechanism (MCM) (Sommariva et al., 2020). The MCM, one of most
87 widely used chemical mechanism for chemistry, is a near-explicit chemical mechanism which describes the degradation of
88 methane and 142 nonmethane VOCs and over 17000 elementary reactions of 6700 primary, secondary and radical species
89 (<http://mcm.york.ac.uk/>, last access: 16 January 2023) (Jenkin et al., 2003; Saunders et al., 2003). AtChem2 software and
90 documentation can be found on <https://github.com/AtChem/> (last accessed on January 16, 2023).

91 In this study, the observed data of O₃, NO₂, SO₂, HONO, HCHO, NMVOCs, $j(\text{NO}_2)$, P, T, RH, and BLH were used as inputs to
92 constrain the model calculations. The photolysis rates of other molecules such as O₃, HCHO, HONO, and OVOCs can be
93 calculated in this model platform with the basic principle driven by the solar zenith angle and scaled by the measured J_{NO_2}
94 (Sommariva et al., 2020). The removal of all unconstrained and simulated species caused by the deposition is determined by a
95 parameterization approach, and is determined by the accumulation of the deposition velocity of 0.01 m s⁻¹ within the boundary
96 layer (Santiago et al., 2017). The sensitivity of simulation results to the deposition velocity has been studied in previous research,
97 and the impact is limited (Zhu et al., 2020). The model outputs include the concentration of the hydroxyl radical (OH) and
98 hydroperoxy radical (HO₂), as well as the reaction rates at each step of the simulation process.

99 2.3 Machine learning

100 Two machine learning methods, k-means clustering and the stacking model, were utilized in this study. In order to investigate the
101 reasons for the overall increase in ozone levels during the static management period from the perspective of its diurnal variation,
102 the k-means clustering method was applied to cluster 24-hour time series of O₃ concentration (Zhang et al., 2004). Time-series
103 clustering is a specific application of curve clustering, which is similar to trajectory clustering in the transport of air masses
104 (Darby, 2005; Suris et al., 2022). The procedure for k-means clustering is as follows: (i) randomly initialize k clusters and then
105 calculate the cluster centroid or mean, (ii) assign each data point to the nearest cluster using an appropriate distance measure, (iii)
106 re-calculate the cluster centroids based on the current cluster members, (iv) repeat steps ii and iii until there is no further change.
107 Additionally, the stacking model was applied to address missing values in DOAS observations caused by uncontrollable factors,
108 ensuring the continuity and variation characteristics of the data. This step was deemed necessary for two main reasons. Firstly,
109 the clustering analysis of O₃ diurnal variation demands a continuous time series without any missing values. Secondly, compared
110 to the conventional method of handling missing data in the input of the OBM model through simple linear interpolation, the
111 stacking model preserves the diurnal variation characteristics of the data, ensuring the correct constraints on the OBM model.
112 The stacked model is an ensemble machine learning algorithm that consists of two levels, with two or more base models at level

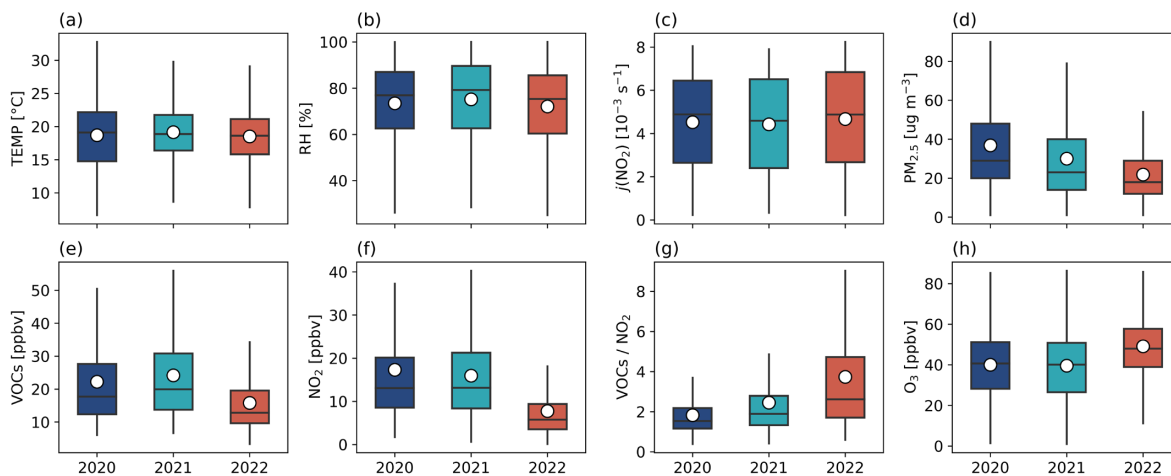


113 0 and one meta-model at level 1. The meta-model is trained using predictions made by the base models on out-of-sample data. In
114 other words, data that was not used to train the base models is fed into them to make predictions. These predictions, along with
115 the corresponding expected outputs, form the input and output pairs of the training dataset used to fit the meta-model. The
116 stacking model has been previously described in detail and demonstrated good performance in Zhu et al. (2022), and the
117 architecture of the stacking model can also be found in Figure S1. In this study, the models for O₃, NO₂, SO₂, HONO, and
118 HCHO demonstrated good performance, as shown in Figure S2-S6 of the Supplement.

119 3 Results and Discussion

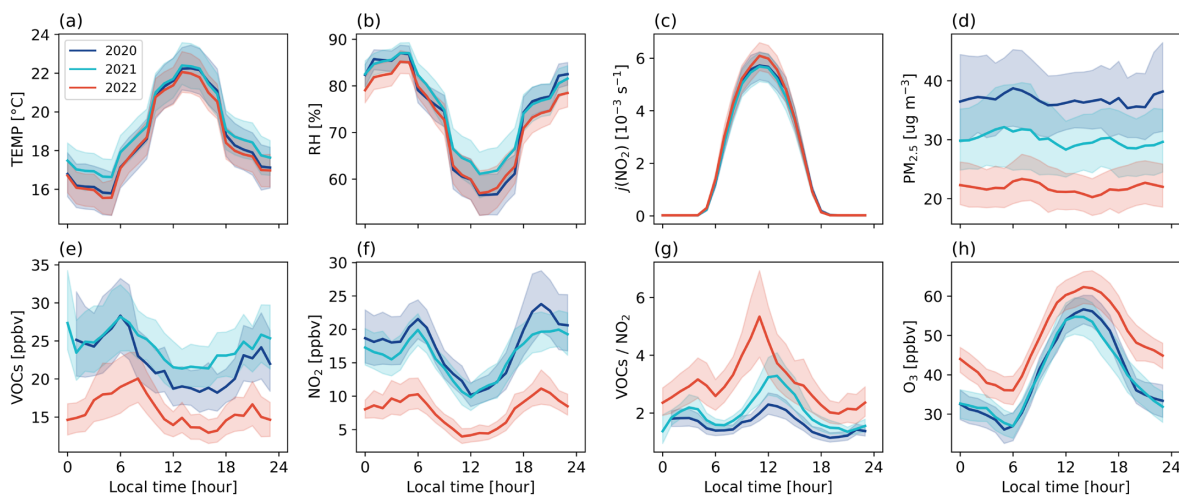
120 3.1 Year-on-year changes on air quality

121 Figure 1 compares the average levels of the meteorological parameters and air pollutants during the period from April to May of
122 2020 to 2022, while Figure 2 compares the diurnal variations. In terms of meteorological parameters, the temperature and
123 relative humidity, and $j(\text{NO}_2)$ during the static management period in 2022 were almost unchanged compared to the same period
124 in 2020 and 2021. The average temperature difference in 2022 was 6.5°C, which was similar to that of 2020 and slightly higher
125 than that of 2021, while the average relative humidity at noon in 2022 was also comparable to that of 2020 and was 5% lower
126 than that of 2021. Furthermore, we also ruled out the contribution of transport from the surrounding areas to the increase in
127 ozone concentration in Shanghai during the 2022 static management period (see Figure S7 and S8). The abrupt reduction of
128 emissions across the entire industry led to a significant decrease in primary pollutant concentrations. The average concentrations
129 of PM_{2.5} in April and May from 2020 to 2022 were 36.8±24.1 ug m⁻³, 30.0±23.1 ug m⁻³, and 21.8±14.0 ug m⁻³, respectively,
130 showing a decreasing trend over the years. And the diurnal variation profile in Figure 2d shows that PM_{2.5} levels decreased
131 proportionally throughout the entire 24-hour period, without any particularly prominent periods of decrease. The VOCs and NO₂
132 declined by 29% and 55% respectively compared to 2020, and by 35% and 51% respectively compared to 2021. Due to the
133 significant decrease in NO₂ concentration compared to VOCs, the average ratio of VOCs/NO₂ has increased from 1.6 in 2020 to
134 3.0 in 2022. However, the precursor reduction at different magnitudes has led to an increase of approximately 23% in the
135 average level of ozone. The photochemical production of ozone is controlled by the non-linear chemistry of the precursors VOCs
136 and NO_x (NO₂+NO). The literatures have shown that Shanghai in the spring largely operates under VOCs-limited regime (Li et
137 al., 2021a; Xue et al., 2022). Therefore, the reduction in VOCs during the static management period may not be enough to
138 counteract the titration effect of NO_x, and may even alter the ozone formation regime in Shanghai. From the perspective of
139 diurnal variation (see Figure 2), the period with a significant difference in the magnitude of the decrease between VOCs and NO₂
140 occurred during the strong photochemical process in the morning until noon. Therefore, the VOCs/NO₂ ratio during the static
141 management period was significantly higher in the morning compared to the same period in 2020 and 2021. The weakening of
142 the titration of nitrogen oxides on ozone during nighttime led to significantly higher nighttime average levels during the static
143 management period compared to 2020 and 2021. Due to the higher O₃ baseline concentration and higher VOCs/NO₂ ratio, there
144 was a significant increase in overall ozone levels.



145

146 **Figure 1. Comparison of meteorological parameters (TEMP, RH, $j(\text{NO}_2)$) and air pollutants ($\text{PM}_{2.5}$, VOCs, NO_2 , VOCs/NO_2 , O_3)**
147 **during the periods from April to May of 2020, 2021, and 2022. The top and bottom of the vertical line for each box correspond to the**
148 **95th and 5th percentiles, respectively. The dots represent the averages, and the top, middle, and bottom lines of the box mark the 75th,**
149 **50th, and 25th percentiles, respectively.**



150

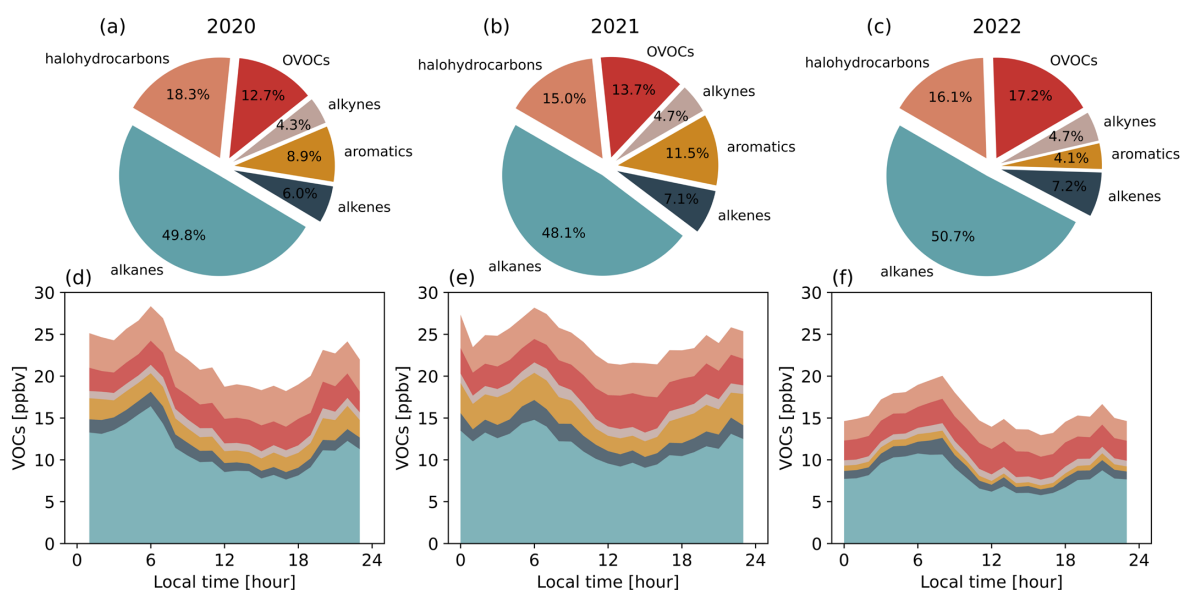
151 **Figure 2. The mean diurnal profiles of meteorological parameters and air pollutants during the periods from April to May of 2020,**
152 **2021, and 2022. Colored areas denote 95% confidence intervals.**

153 As VOCs are crucial precursors for ozone formation, we conducted a comparison of each VOCs component during the 2022
154 static management period with those of the same period in 2020 and 2021, as shown in Figure 3. We classified the 103 VOCs
155 into six categories, including alkanes, alkenes, alkynes, aromatics, oxygenated VOCs (OVOCs), and halohydrocarbons. The
156 detailed classification is available in the Table S2. The results revealed that aromatics experienced the most significant year-
157 over-year reduction in absolute terms. The chemical raw materials and chemical products manufacturing industry, which is the
158 main source of aromatics (Liu et al., 2019), accounts for 10% of the total industrial output value, and this industry experienced a
159 32% year-on-year decrease in total output value during the static management period. In contrast, OVOCs remained relatively
160 stable, primarily because they are sourced from biogenic (Liu et al., 2019), and thus, were less impacted by lockdown measures
161 relative to other VOCs.



162 The reduction in the imbalance of VOCs has altered the average proportion of each component. Specifically, the proportion of
163 aromatics decreased from 8.9% and 11.5% to 4.1%, while the proportion of OVOCs increased from 12.7% and 13.7% to 17.2%.
164 The photolysis of OVOCs is a major source of the important radicals ROx (OH+HO₂+RO₂) in the photochemical cycle, with a
165 daily average contribution rate of over 30% (Xue et al., 2016). Consequently, the rise in OVOC proportion during the static
166 management period has the potential to enhance the photochemical process. The mean diurnal profiles of the VOCs indicated
167 that the daily average concentration range in 2020, 2021, and 2022 was between 18-28 ppbv, 21-28 ppbv, and 13-20 ppbv,
168 respectively.

169 In 2022, the peak time of VOCs was observed at 08:00, which exhibited a delay compared to the peak times observed in 2020
170 and 2021 at 06:00, resembling the previously reported “weekend effect” on VOCs that the peak time of VOCs is delayed on
171 weekends in comparison to weekdays (Cai et al., 2010). This finding indicates that the reduced human activities during the 2022
172 period, similar to weekends, led to a decline in anthropogenic VOC emissions in the morning.



173
174 **Figure 3. The proportions (a, b, c) and the mean diurnal profiles (d, e, f) of different VOCs components during the periods from April**
175 **to May of 2020, 2021, and 2022.**

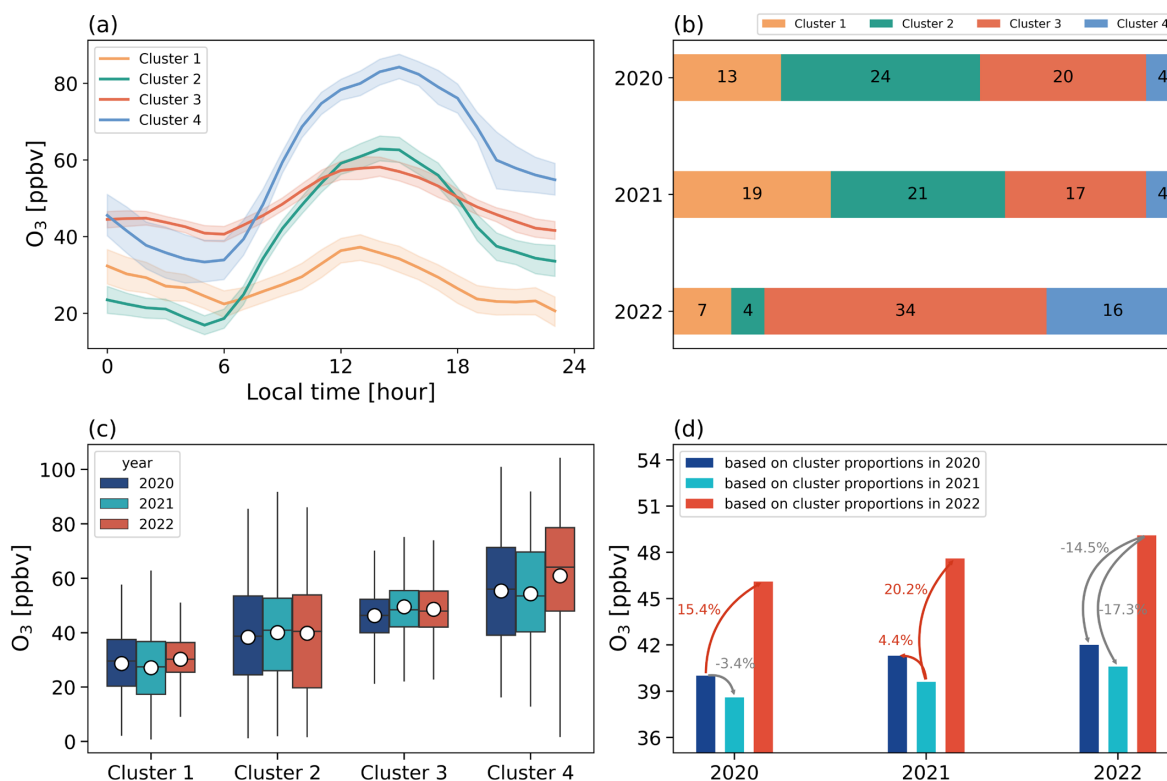
176

177 3.2 Clustering of O₃ diurnal profiles

178 The k-means algorithm clustered the ozone diurnal profiles over the three years into four types, as shown in Figure 4a. These
179 four types of profiles can be described as follows: Cluster 1 with low background concentration and low net production; Cluster
180 2 with low background concentration and high net production; Cluster 3 with high background concentration and low net
181 production; and Cluster 4 with high background concentration and high net production. The background concentration of ozone
182 is mainly determined by the nighttime loss of ozone and the titration of nitrogen oxides in the morning, while the net production
183 depends on the intensity of the photochemical reactions. In Figure 4b, the four ozone profiles occurred for 13, 24, 20, and 4 days
184 in 2020, comparable occupation of 19, 21, 17, and 4 days in 2021, respectively. During the static management period of 2022,
185 when the nitrogen oxide titration effect weakened, the number of days on which Cluster 3 and Cluster 4 appeared increased to 34
186 and 16, respectively. The average ozone levels for the four types were comparable across 2020, 2021, and 2022, ranging from



187 27-30 ppbv for Cluster 1, 38-40 ppbv for Cluster 2, 46-49 ppbv for Cluster 3, and 54-61 ppbv for Cluster 4 (Figure 4c). As
 188 depicted in Figure 4d, assuming that the proportions of the four types in 2022 are the same as those in 2020 and 2021, the
 189 average ozone levels in 2022 would decrease by 14.5% and 17.3%, respectively, remaining comparable to the levels in 2020 and
 190 2021. Alternatively, if the proportions of the four types in 2020 and 2021 were the same as those in 2022, the average ozone
 191 levels in 2020 and 2021 would increase by 15.4% and 20.2%, respectively, which would be very close to the levels in 2022.
 192 Purely statistical analysis indicated that the significant increase in ozone levels in 2022 was due to a higher proportion of Cluster
 193 3 and Cluster 4, which had higher ozone concentrations during the static management period.

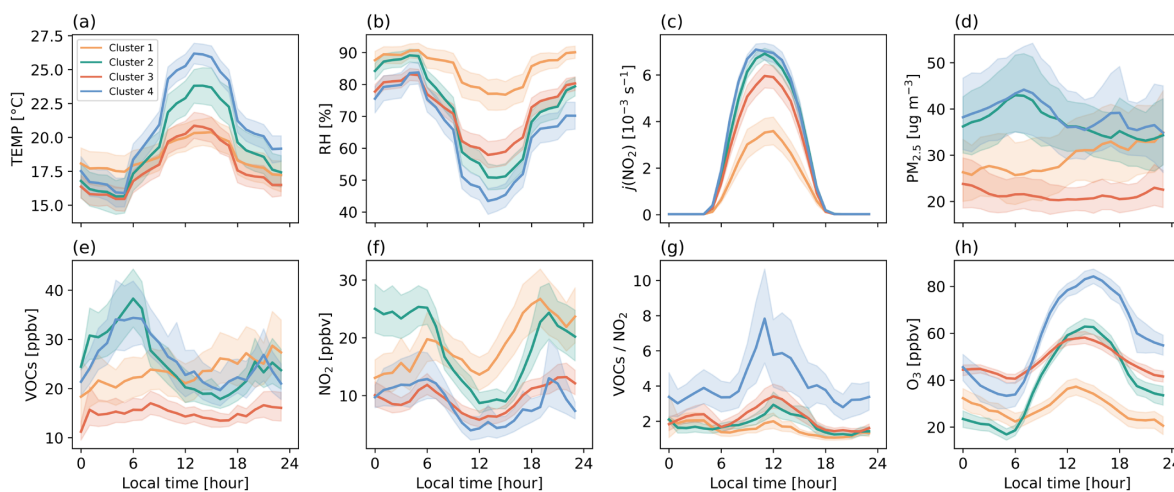


194
 195 **Figure 4. (a) Comparison of the mean diurnal profiles of the four types of O₃ after clustering. Colored areas denote 95% confidence**
 196 **intervals; (b) The proportions of the four clusters in 2020, 2021 and 2022. (c) Comparison of the O₃ levels of the four clusters in 2020,**
 197 **2021 and 2022. The top and bottom of the vertical line for each box correspond to the 95th and 5th percentiles, respectively. The dots**
 198 **represent the averages, and the top, middle, and bottom lines of the box mark the 75th, 50th, and 25th percentiles, respectively; (d)**
 199 **Comparison of the average ozone concentrations in 2020, 2021 and 2022 for different ratios of the four clusters.**

200 Different types of ozone profiles are formed under different meteorological conditions and pollution environments with
 201 distinctive diurnal variations. The meteorological conditions during the periods of Cluster 2 and Cluster 4, with high net ozone
 202 production, were characterized by high temperature, low relative humidity, and high radiation, compared to those during Cluster
 203 1 and Cluster 3 periods. This is consistent with the well-known favorable condition promoting ozone production. The valley
 204 values of ozone profiles are closely related to the titration of nitrogen oxides, as shown in Figures 5f and 5h, where the valley
 205 values of ozone are inversely related to the peak values of NO₂ during the morning rush hour. Indeed, it is these meteorological
 206 conditions and titration that result in the formation of the corresponding four clusters of ozone profiles. During periods of Cluster
 207 2 and Cluster 4, a large amount of VOCs accumulated before sunrise and were rapidly consumed after sunrise. Similarly, the
 208 precursor NO₂ was also rapidly consumed after sunrise, with the difference that the NO₂ level during Cluster 4 was lower than



209 that of Cluster 2. The VOCs/NO₂ ratio in Cluster 4 was significantly higher than that in other clusters, which may explain the
210 substantial net ozone production despite the relatively high ozone background levels. The differences among the clusters are also
211 reflected in the photochemical processes. In the following sections, we investigated the reasons for the increase in ozone levels
212 during the static management period from the perspective of atmospheric oxidizing capacity and free radical chemistry.



213

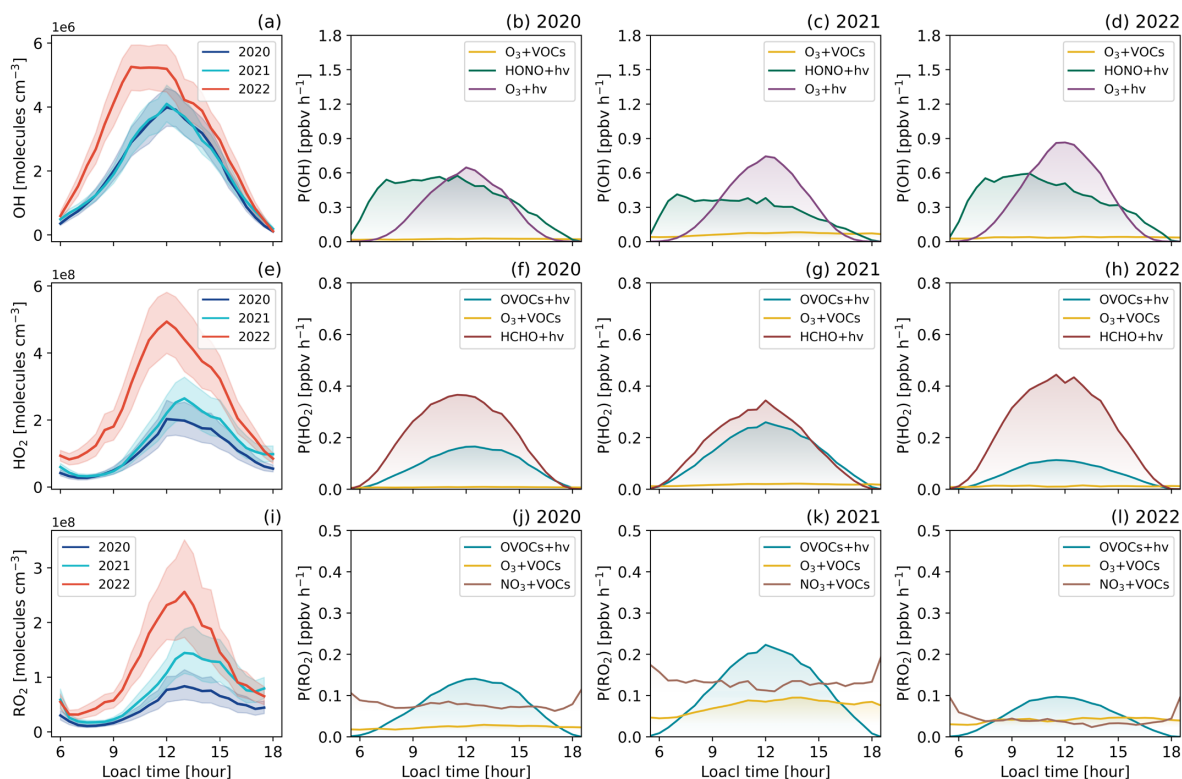
214 **Figure 5. The mean diurnal profiles of meteorological parameters and air pollutants for four clusters over three years. Colored areas**
215 **denote 95% confidence intervals.**

216 3.3 Radical chemistry

217 Figures 6a, 6e and 6i show the mean diurnal profiles of simulated OH, HO₂ and RO₂ radical concentrations for the years 2020,
218 2021, and 2022. These radicals exhibit clear diurnal variations, with peaks occurring at midday. The mean diurnal profiles
219 display that the average peak concentrations of OH were 4.0×10^6 , 4.1×10^6 , and 5.3×10^6 , those of HO₂ were 2.0×10^8 , $2.6 \times$
220 10^8 , and 4.9×10^8 molecules cm⁻³, and those of RO₂ were 0.8×10^8 , 1.4×10^8 and 2.6×10^8 molecules cm⁻³, respectively.
221 Reviewing previously observational results, peak concentrations of OH and HO₂ were observed at various locations and times:
222 $(4-17) \times 10^6$ molecules cm⁻³ and $(2-24) \times 10^8$ molecules cm⁻³ at a suburban site in Yufa from Aug 18-31, 2006 (Lu et al., 2013);
223 $(5-15) \times 10^6$ molecules cm⁻³ and $(3-14) \times 10^8$ molecules cm⁻³ at a rural site in Wangdu from June 8 to July 8, 2014 (Tan et al.,
224 2017); 4.5×10^6 molecules cm⁻³ and 3×10^8 molecules cm⁻³ at a suburban in Heshan from October 22 to November 5, 2014 (Tan
225 et al., 2019); $(2-9) \times 10^6$ molecules cm⁻³ and $(2-14) \times 10^8$ molecules cm⁻³ at a urban sites in Shenzhen from Oct 5-28, 2018 (Yang
226 et al., 2022); $(8-24) \times 10^6$ molecules cm⁻³ and $(4-28) \times 10^8$ molecules cm⁻³ at a suburban site in Taizhou from May 23 to June 18,
227 2018 (Ma et al., 2022); and $(10-20) \times 10^6$ molecules cm⁻³ and $(6-18) \times 10^8$ molecules cm⁻³ at a suburban site in Chengdu from
228 Aug 10-25, 2019 (Yang et al., 2021). The simulated concentrations of OH and HO₂ in this study were comparable to the
229 observed levels during autumn in Shenzhen, which is also an urban site, however, were generally lower than those observed at
230 non-urban sites. This difference can be attributed to the site types, but more importantly, to the fact that most observations were
231 conducted during periods of stronger radiation. For RO₂, the average maximum concentration was simulated to be 4.5×10^8
232 molecules cm⁻³ at urban site of Beijing in August 2007. At coastal site of Xiamen, the simulated average daily peak reached 4.7
233 $\times 10^8$ molecules cm⁻³ in September 2019, while at the coastal site of Ningde, the simulated value was 0.9×10^8 molecules cm⁻³ in
234 spring 2019. Overall, our ROx concentrations fell within the range of observations and simulated results in other regions of
235 China. During the static management period in 2022, the levels of ROx were significantly higher compared to the same period in
236 2020 and 2021, indicating an enhanced atmospheric oxidation capacity in Shanghai in 2022.



237 Figures 6b-6d, Figures 6f-6h, and Figures 6j-6l illustrate the mean diurnal variation of primary OH, HO₂, and RO₂ sources for
238 the years of 2020, 2021, and 2022. For OH, HONO photolysis peaked at around 07:00 and remained high until around 12:00,
239 with peak values reaching approximately 0.57 ppbv h⁻¹, 0.41 ppbv h⁻¹, and 0.59 ppbv h⁻¹ in 2020, 2021, and 2022, respectively.
240 Meanwhile, ozone photolysis peaked at noon, with peak values reaching around 0.65 ppbv h⁻¹, 0.74 ppbv h⁻¹, and 0.87 ppbv h⁻¹,
241 respectively. In addition, the ozonolysis of unsaturated VOCs was another source of OH radical, with an average production rate
242 of less than 0.10 ppbv h⁻¹, while other sources such as the photolysis of H₂O₂, HNO₃, and OVOCs were generally negligible.
243 Overall, HONO photolysis for the daytime accounted for 57%, 42%, and 48% of the total OH primary production rates in 2020,
244 2021, and 2022, respectively, with O₃ photolysis accounting for 40%, 48%, and 47% in the corresponding years. For HO₂ radical,
245 the most important source was HCHO photolysis, with average production rates during daytime of 0.20 ppbv h⁻¹, 0.17 ppbv h⁻¹,
246 and 0.24 ppbv h⁻¹ in the corresponding years, respectively. The secondary source was OVOCs photolysis, which produce HO₂ at
247 the rate of 0.10 ppbv h⁻¹, 0.15 ppbv h⁻¹, and 0.06 ppbv h⁻¹, respectively. Another source to consider was reactions of O₃ and
248 unsaturated VOCs, which has an average rate of around 0.02 ppbv h⁻¹. For RO₂ radical, the daytime average peak of primary
249 production rates contributed by OVOCs photolysis from 2020 to 2022 were 0.14 ppbv h⁻¹, 0.22 ppbv h⁻¹, and 0.10 ppbv h⁻¹,
250 respectively. The reactions of O₃ and NO₃ with VOCs were also important primary sources of RO₂ radical. The average daily
251 contributions of O₃+VOC reactions from 2020 to 2022 were 0.02 ppbv h⁻¹, 0.08 ppbv h⁻¹, and 0.04 ppbv h⁻¹, while the
252 contributions of NO₃+VOC reactions were 0.08 ppbv h⁻¹, 0.13 ppbv h⁻¹, and 0.04 ppbv h⁻¹, respectively. The primary production
253 rate of RO₂ in 2022 was lower compared to the years 2020 and 2021. This can be attributed to the fact that the primary sources of
254 RO₂ are the reactions involved VOCs, which significantly decreased during the static management period and further led to the
255 decreased sources of RO₂.
256 Overall, the primary production rates of RO_x remained relatively stable from 2020 to 2022, with values of 1.20 ppbv h⁻¹, 1.35
257 ppbv h⁻¹, and 1.28 ppbv h⁻¹, respectively. These values are close to the simulated value of 1.56 ppbv h⁻¹ in November 2019 in
258 downtown Shanghai (Zhang et al., 2022a), but lower than the value of 2.55 ppbv h⁻¹ during the ozone episode in the suburban of
259 Shanghai in 2018 (Zhang et al., 2021). During these three years, reactions involving VOCs (excluding HCHO) accounted for
260 25%, 42%, and 19%, respectively, which is correlated with the observed VOCs abundances. In 2020 and 2022, HONO
261 photolysis accounted for over 30% of the total primary production rates, followed by O₃ photolysis, which accounted for 23%
262 and 30% respectively. In 2021, the dominant contribution was from O₃ photolysis, reaching 24%, followed by HONO photolysis
263 at 20%. Radical chemistry exhibits heterogeneity across different cities, with HONO photolysis being a primary source in New
264 York (Ren et al., 2003), Paris (Michoud et al., 2012), Wangdu (Tan et al., 2017), and Taizhou (Ma et al., 2022). OVOC
265 photolysis dominated in Mexico City (Sheehy et al., 2010), Hong Kong (Xue et al., 2016), and Beijing (Liu et al., 2012). Milan
266 relied on HCHO photolysis as a major source (Alicke et al., 2002), while ozone photolysis was prominent in Nashville (Martinez
267 et al., 2003).
268

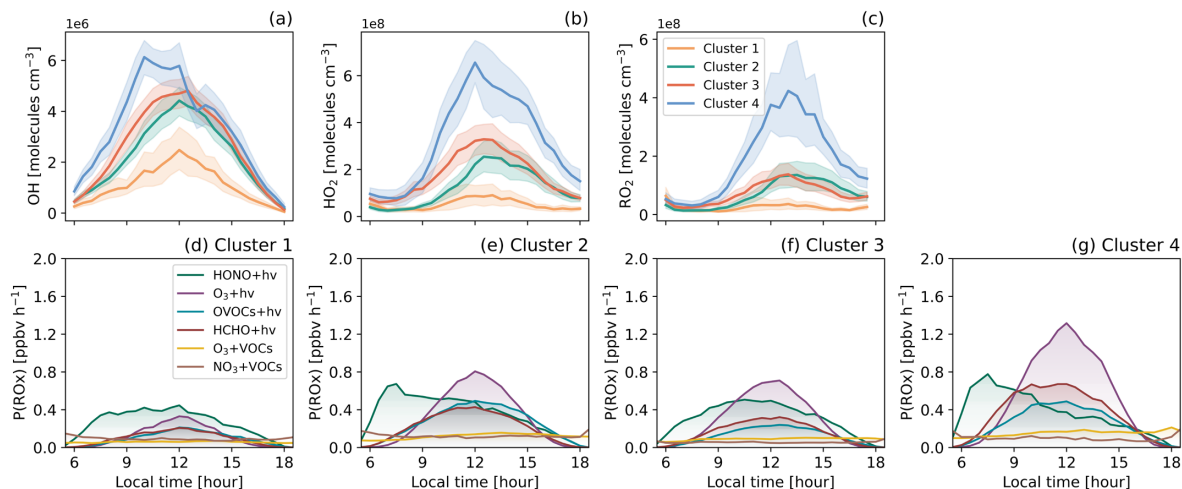


269

270 **Figure 6. The mean diurnal profiles of simulated OH (a), HO₂ (e), and RO₂ (i) concentrations in 2020, 2021, and 2022. Colored areas**
 271 **denote 95% confidence intervals; The mean diurnal profiles of primary sources of OH radical (b-d) , HO₂ radical (f-h), and RO₂**
 272 **radical (j-l) from model calculations in 2020, 2021 and 2022.**

273 We also investigated the radical chemistry under different ozone profile clusters (Figure 7). The average peak of OH in Cluster 1,
 274 Cluster 2, Cluster 3, and Cluster 4 were 2.5×10^6 molecules cm^{-3} , 4.4×10^6 molecules cm^{-3} , 4.8×10^6 molecules cm^{-3} , and $6.1 \times$
 275 10^6 molecules cm^{-3} , those of HO₂ were 0.9×10^8 molecules cm^{-3} , 2.5×10^8 molecules cm^{-3} , 3.3×10^8 molecules cm^{-3} , and $6.6 \times$
 276 10^8 molecules cm^{-3} , and those of RO₂ were 0.4×10^8 molecules cm^{-3} , 1.3×10^8 molecules cm^{-3} , 1.4×10^8 molecules cm^{-3} , and
 277 4.2×10^8 molecules cm^{-3} , respectively. The order of those concentrations among the four clusters is consistent with the order of
 278 average ozone concentration. Cluster 2 and Cluster 4, characterized by significant net ozone production, exhibit distinct features
 279 in radical chemistry. The daily average of P(ROx) was 1.50 ppbv h^{-1} in Cluster 2 and 1.89 ppbv h^{-1} in Cluster 4, which is higher
 280 than the values of 0.78 ppbv h^{-1} in Cluster 1 and 1.11 ppbv h^{-1} in Cluster 3. In addition, HONO photolysis during the morning
 281 rush hour was particularly prominent in Cluster 2 and Cluster 4, with peak values reaching 0.67 ppbv h^{-1} and 0.78 ppbv h^{-1} ,
 282 respectively. In Cluster 2, HONO photolysis was the dominant source with a daily average of 0.40 ppbv h^{-1} , accounting for 26%
 283 of the total, and ozone photolysis followed with 0.34 ppbv h^{-1} , accounting for 23%. On the other hand, in Cluster 4, ozone
 284 photolysis took the lead with 0.58 ppbv h^{-1} , representing 30% of the total, and HONO photolysis came next with 0.40 ppbv h^{-1} ,
 285 accounting for 21%. Additionally, OVOCs photolysis (including HCHO) in Cluster 2 and Cluster 4 showed a significant increase
 286 compared to Cluster 1 and Cluster 3. In conclusion, a large amount of net ozone production implies the presence of active
 287 photochemical processes.

288



289
290

Figure 7. The mean diurnal profiles of simulated OH (a), HO₂ (b), and RO₂ (c) concentrations for Cluster 1, Cluster 2, Cluster 3, and Cluster 4. Colored areas denote 95% confidence intervals; The mean diurnal profiles of primary sources of ROx radical (d-g) from model calculations for Cluster 1, Cluster 2, Cluster 3, and Cluster 4.

291

292

293

294

295

296

297

298

299

300

301

302

303

304

305

306

307

308

309

310

311

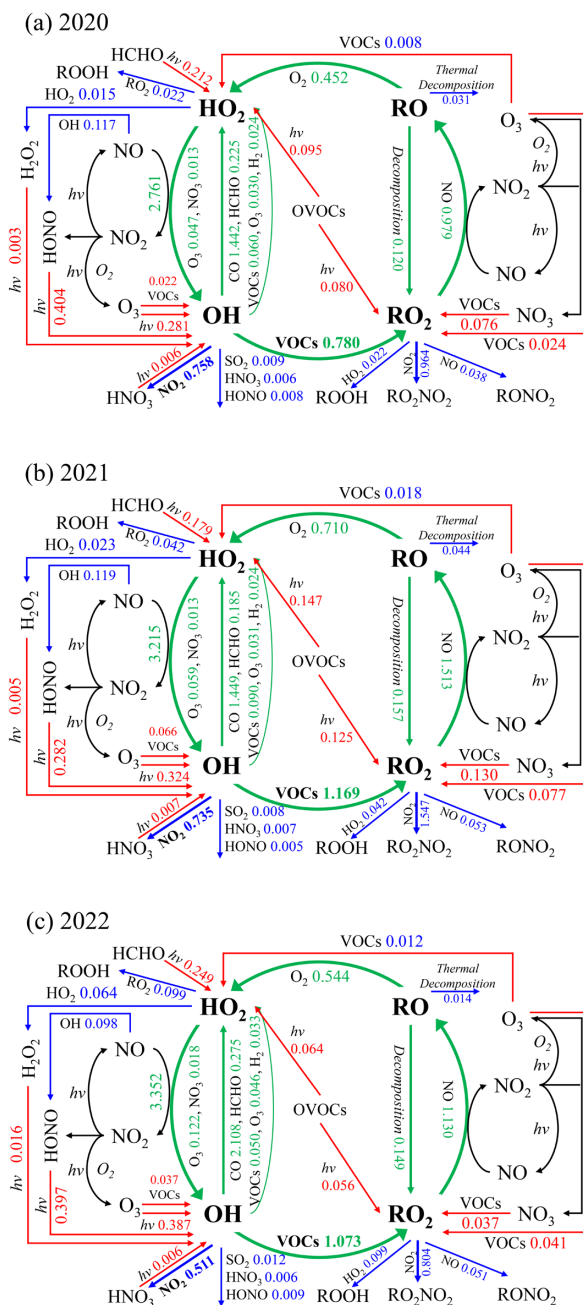
312

313

314

315

In tropospheric chemistry, radical initiation, which involves the breakdown of closed-shell species to generate new radicals, plays a crucial role in initiating the formation of secondary pollutants. However, in highly polluted atmospheric environments, radical cycling becomes the dominant process, with the amplification of new radicals in the ROx cycle playing a crucial role. Volkamer et al. (2010) quantified the production of new radicals and found that approximately 20% of radical production is attributed to the breakdown of closed-shell species, while 80% is derived from radical cycling. Therefore, in addition to understanding the sources of radicals, it is essential to comprehend the impacts of radical cycling and recycling processes on ozone formation. Figure 8 demonstrated the daytime average of ROx radicals budgets during the periods from April to May of 2020, 2021, and 2022. Taking the simulation of 2022 as an example, OH oxidation of CO and VOCs produces HO₂ and RO₂ with daytime average rates of 2.11 ppbv h⁻¹ (1.44 ppbv h⁻¹ in 2020 and 1.45 ppbv h⁻¹ in 2021) and 1.07 ppbv h⁻¹ (0.78 ppbv h⁻¹ in 2020 and 1.17 ppbv h⁻¹ in 2021), respectively. The reactions of RO₂+NO and HO₂+NO further lead to the strong production of RO with a rate of 1.13 ppbv h⁻¹ (0.98 ppbv h⁻¹ in 2020 and 1.51 ppbv h⁻¹ in 2021) and OH with a rate of 3.35 ppbv h⁻¹ (2.76 ppbv h⁻¹ in 2020 and 3.22 ppbv h⁻¹ in 2021), while generating O₃ as a by-product. Clearly, these recycling processes dominate the overall production of ROx radicals compared to the primary sources. In terms of termination processes, the loss of ROx radicals was primarily dominated by their reactions with NOx. Specifically, the reactions of OH+NO₂ and RO₂+NO₂ accounted for approximately 0.51 ppbv h⁻¹ (0.76 ppbv h⁻¹ in 2020 and 0.74 ppbv h⁻¹ in 2021) and 0.80 ppbv h⁻¹ (0.96 ppbv h⁻¹ in 2020 and 1.55 ppbv h⁻¹ in 2021) of the ROx radical loss on daytime average, respectively. This is in line with the understanding that reactions involving NOx typically play a dominant role in the removal of radicals in high NOx environments (Zhang et al., 2021; Xue et al., 2016; Volkamer et al., 2010; Tan et al., 2019; Liu et al., 2012). To sum up, the changes resulting from the approximately 55% reduction in NO₂ and 30% reduction in VOCs due to static management are reflected in both the radical propagation and termination processes. The ratio of OH radical propagation (OH+VOCs) to termination (OH+NO₂) reached 2.10, which is higher than 1.03 in 2020 and 1.60 in 2021. It can be interfered the different proportions of NO₂ and VOCs reduction did not weaken the radical cycling. On the contrary, a higher VOCs/NO₂ ratio promotes the radical recycling efficiency in the reaction chain of radicals.



316
 317 **Figure 8.** Averaged budgets (in ppbv h⁻¹) of ROx radicals in daytime (06:00-18:00) during the periods from April to May of 2020, 2021,
 318 and 2022. The red, blue, and green lines and words indicate the primary production, termination, and recycling pathways of radicals,
 319 respectively.

320 **4 Conclusions**

321 The two-month city-wide static management was implemented in April and May 2022 in Shanghai aiming to control the spread
 322 of the Omicron variant, which provides a valuable opportunity to study the causes of ozone pollution. The comprehensive



323 observations during the static management and same period in 2020 and 2021 shows that , there was a decrease of 29%-35% in
324 VOCs and 51%-55% in NO₂ concentrations, while the average ozone level increased by nearly 23%. By statistics, the ozone
325 profiles were classified into four clusters: Cluster 1, characterized by low background concentration and low net production;
326 Cluster 2, characterized by low background concentration and high net production; Cluster 3, characterized by high background
327 concentration and low net production; and Cluster 4, characterized by high background concentration and high net production.
328 The average concentration relationship among these clusters is Cluster 4 > Cluster 3 > Cluster 2 > Cluster 1. The significant
329 increase in the proportion of Cluster 4 and Cluster 3 during the period of static management resulted in the overall increase in the
330 average ozone level. Secondly, from the perspective of radical chemistry, we explored the changes in photochemical processes
331 due to the reduction in precursor species. The OBM model simulated the levels of radicals and their processes of initiation,
332 propagation, and termination. The average peak concentrations of OH, HO₂, and RO₂ in 2022 were 5.3×10^6 , 4.9×10^8 , and 2.6
333 $\times 10^8$ molecules cm⁻³, respectively, which were higher than those in the same period in 2020 and 2021. HONO photolysis was
334 the main contributor to the primary source of RO_x, accounting for about 30% of the total. However, in terms of the overall
335 production of RO_x radicals, the radical recycling process remained dominant. The reduction of NO₂ and VOCs in different
336 proportions due to static management has led to an increased ratio of OH radical propagation (OH+VOCs) to termination
337 (OH+NO₂), reaching 2.10, which is higher than 1.03 in 2020 and 1.60 in 2021. This enhanced ratio indicates a strengthened
338 radical cycling as a result of a higher VOCs/NO₂ ratio.

339 The important lesson we learned from the “large-scale field experiment” during the period of static management is that Shanghai
340 is in VOCs-limited regime. When the reduction in VOCs is not able to catch up with or exceed the reduction in nitrogen oxides,
341 it is not sufficient to curb the formation of secondary pollutants. In terms of ozone control strategies, it is necessary to strengthen
342 the regulation and control of VOCs.

343 **Data Availability**

344 The observed and predicted hourly time series data in the study are presented in Figure S11-S12, and Code and data used for our
345 analyses are available at <https://data.mendeley.com/datasets/3kmhg7r2df/1>(Zhu, 2023).

346 **Competing interests**

347 The contact author has declared that none of the authors has any competing interests.

348 **Author contributions**

349 Jian Zhu: Conceptualization, Methodology, Software, Validation, Investigation, Writing original draft, Visualization. Shanshan
350 Wang: Conceptualization, Methodology, Supervision, Funding acquisition. Chuanqi Gu, Zhiwen Jiang, Sanbao Zhang, Ruibin
351 Xue, and Yuhao Yan: Methodology, Validation, Investigation. Bin Zhou: Conceptualization, Methodology, Supervision,
352 Funding acquisition.

353 **Acknowledgments**

354 This work was supported by National Natural Science Foundation of China (22176037, 42075097, 22376030, 42375089,
355 21976031) and National Key Research and Development Program of China (2022YFC3700101).
356



357 References

- 358 Agarwal, A., Kaushik, A., Kumar, S., and Mishra, R. K.: Comparative study on air quality status in Indian and Chinese cities
359 before and during the COVID-19 lockdown period, *Air Quality, Atmosphere & Health*, 13, 1167-1178,
360 <https://doi.org/10.1007/s11869-020-00881-z>, 2020.
- 361 Aliche, B., Platt, U., and Stutz, J.: Impact of nitrous acid photolysis on the total hydroxyl radical budget during the Limitation of
362 Oxidant Production/Pianura Padana Produzione di Ozono study in Milan, *Journal of Geophysical Research: Atmospheres*, 107,
363 LOP 9-1-LOP 9-17, <https://doi.org/10.1029/2000JD000075>, 2002.
- 364 Bao, R. and Zhang, A.: Does lockdown reduce air pollution? Evidence from 44 cities in northern China, *Science of the Total
365 Environment*, 731, 139052, <https://doi.org/10.1016/j.scitotenv.2020.139052>, 2020.
- 366 Cai, C., Geng, F., Tie, X., Yu, Q., and An, J.: Characteristics and source apportionment of VOCs measured in Shanghai, China,
367 *Atmospheric Environment*, 44, 5005-5014, <https://doi.org/10.1016/j.atmosenv.2010.07.059>, 2010.
- 368 Chu, B., Zhang, S., Liu, J., Ma, Q., and He, H.: Significant concurrent decrease in PM_{2.5} and NO₂ concentrations in China during
369 COVID-19 epidemic, *Journal of Environmental Sciences*, 99, 346-353, <https://doi.org/10.1016/j.jes.2020.06.031>, 2021.
- 370 Darby, L. S.: Cluster analysis of surface winds in Houston, Texas, and the impact of wind patterns on ozone, *Journal of Applied
371 Meteorology and Climatology*, 44, 1788-1806, <https://doi.org/10.1175/JAM2320.1>, 2005.
- 372 Gu, C., Wang, S., Zhu, J., Wu, S., Duan, Y., Gao, S., and Zhou, B.: Investigation on the urban ambient isoprene and its oxidation
373 processes, *Atmospheric Environment*, 270, 118870, <https://doi.org/10.1016/j.atmosenv.2021.118870>, 2022.
- 374 Guo, Y., Wang, S., Zhu, J., Zhang, R., Gao, S., Saiz-Lopez, A., and Zhou, B.: Atmospheric formaldehyde, glyoxal and their
375 relations to ozone pollution under low-and high-NO_x regimes in summertime Shanghai, China, *Atmospheric Research*, 258,
376 105635, <https://doi.org/10.1016/j.atmosres.2021.105635>, 2021.
- 377 Hua, J., Zhang, Y., de Foy, B., Shang, J., Schauer, J. J., Mei, X., Sulaymon, I. D., and Han, T.: Quantitative estimation of
378 meteorological impacts and the COVID-19 lockdown reductions on NO₂ and PM_{2.5} over the Beijing area using Generalized
379 Additive Models (GAM), *Journal of Environmental Management*, 291, 112676, <https://doi.org/10.1016/j.jenvman.2021.112676>,
380 2021.
- 381 Huang, X., Ding, A., Gao, J., Zheng, B., Zhou, D., Qi, X., Tang, R., Wang, J., Ren, C., and Nie, W.: Enhanced secondary
382 pollution offset reduction of primary emissions during COVID-19 lockdown in China, *National Science Review*, 8, nwa137,
383 <https://doi.org/10.1093/nsr/nwaa137>, 2021.
- 384 Jenkin, M., Saunders, S., Wagner, V., and Pilling, M.: Protocol for the development of the Master Chemical Mechanism, MCM
385 v3 (Part B): tropospheric degradation of aromatic volatile organic compounds, *Atmospheric Chemistry and Physics*, 3, 181-193,
386 <https://doi.org/10.5194/acp-3-181-2003>, 2003.
- 387 Li, D., Wang, S., Xue, R., Zhu, J., Zhang, S., Sun, Z., and Zhou, B.: OMI-observed HCHO in Shanghai, China, during 2010–
388 2019 and ozone sensitivity inferred by an improved HCHO/NO₂ ratio, *Atmospheric Chemistry and Physics*, 21, 15447-15460,
389 <https://doi.org/10.5194/acp-21-15447-2021>, 2021a.
- 390 Li, R., Zhao, Y., Fu, H., Chen, J., Peng, M., and Wang, C.: Substantial changes in gaseous pollutants and chemical compositions
391 in fine particles in the North China Plain during the COVID-19 lockdown period: anthropogenic vs. meteorological influences,
392 *Atmospheric Chemistry and Physics*, 21, 8677-8692, <https://doi.org/10.5194/acp-21-8677-2021>, 2021b.
- 393 Liu, C. and Shi, K.: A review on methodology in O₃-NO_x-VOC sensitivity study, *Environmental Pollution*, 291, 118249,
394 <https://doi.org/10.1016/j.envpol.2021.118249>, 2021.
- 395 Liu, T., Wang, X., Hu, J., Wang, Q., An, J., Gong, K., Sun, J., Li, L., Qin, M., and Li, J.: Driving forces of changes in air quality
396 during the COVID-19 lockdown period in the Yangtze River Delta Region, China, *Environmental Science & Technology Letters*,
397 7, 779-786, <https://doi.org/10.1021/acs.estlett.0c00511>, 2020.
- 398 Liu, Y., Wang, H., Jing, S., Gao, Y., Peng, Y., Lou, S., Cheng, T., Tao, S., Li, L., and Li, Y.: Characteristics and sources of
399 volatile organic compounds (VOCs) in Shanghai during summer: Implications of regional transport, *Atmospheric Environment*,
400 215, 116902, <https://doi.org/10.1016/j.atmosenv.2019.116902>, 2019.
- 401 Liu, Z., Wang, Y., Gu, D., Zhao, C., Huey, L. G., Stickel, R., Liao, J., Shao, M., Zhu, T., and Zeng, L.: Summertime
402 photochemistry during CAREBeijing-2007: RO_x budgets and O₃ formation, *Atmospheric Chemistry and Physics*, 12, 7737-7752,
403 <https://doi.org/10.5194/acp-12-7737-2012>, 2012.
- 404 Lu, K., Hofzumahaus, A., Holland, F., Bohn, B., Brauers, T., Fuchs, H., Hu, M., Häseler, R., Kita, K., and Kondo, Y.: Missing
405 OH source in a suburban environment near Beijing: observed and modelled OH and HO₂ concentrations in summer 2006,
406 *Atmospheric Chemistry and Physics*, 13, 1057-1080, <https://doi.org/10.5194/acp-13-1057-2013>, 2013.
- 407 Ma, X., Tan, Z., Lu, K., Yang, X., Chen, X., Wang, H., Chen, S., Fang, X., Li, S., and Li, X.: OH and HO₂ radical chemistry at a
408 suburban site during the EXPLORE-YRD campaign in 2018, *Atmospheric Chemistry and Physics*, 22, 7005-7028,
409 <https://doi.org/10.5194/acp-22-7005-2022>, 2022.
- 410 Martinez, M., Harder, H., Kovacs, T., Simpas, J., Bassis, J., Leshner, R., Brune, W., Frost, G., Williams, E., and Stroud, C.: OH
411 and HO₂ concentrations, sources, and loss rates during the Southern Oxidants Study in Nashville, Tennessee, summer 1999,
412 *Journal of Geophysical Research: Atmospheres*, 108, <https://doi.org/10.1029/2003JD003551>, 2003.
- 413 Michoud, V., Kukui, A., Camredon, M., Colomb, A., Borbon, A., Miet, K., Aumont, B., Beekmann, M., Durand-Jolibois, R., and
414 Perrier, S.: Radical budget analysis in a suburban European site during the MEGAPOLI summer field campaign, *Atmospheric
415 Chemistry and Physics*, 12, 11951-11974, <https://doi.org/10.5194/acp-12-11951-2012>, 2012.



- 416 Rana, R. H., Keramat, S. A., and Gow, J.: A systematic literature review of the impact of COVID-19 lockdowns on air quality in
417 China, *Aerosol and Air Quality Research*, 21, 200614, <https://doi.org/10.4209/aaqr.200614>, 2021.
- 418 Ren, X., Harder, H., Martinez, M., Leshner, R. L., Oligier, A., Shirley, T., Adams, J., Simpasa, J. B., and Brune, W. H.: HOx
419 concentrations and OH reactivity observations in New York City during PMTACS-NY2001, *Atmospheric Environment*, 37,
420 3627-3637, [https://doi.org/10.1016/S1352-2310\(03\)00460-6](https://doi.org/10.1016/S1352-2310(03)00460-6), 2003.
- 421 Santiago, J.-L., Martilli, A., and Martin, F.: On dry deposition modelling of atmospheric pollutants on vegetation at the
422 microscale: Application to the impact of street vegetation on air quality, *Boundary-layer meteorology*, 162, 451-474,
423 <https://doi.org/10.1007/s10546-016-0210-5>, 2017.
- 424 Saunders, S. M., Jenkin, M. E., Derwent, R., and Pilling, M.: Protocol for the development of the Master Chemical Mechanism,
425 MCM v3 (Part A): tropospheric degradation of non-aromatic volatile organic compounds, *Atmospheric Chemistry and Physics*, 3,
426 161-180, <https://doi.org/10.5194/acp-3-161-2003>, 2003.
- 427 Sheehy, P., Volkamer, R., Molina, L. T., and Molina, M. J.: Oxidative capacity of the Mexico City atmosphere-Part 2: A ROx
428 radical cycling perspective, *Atmospheric Chemistry and Physics*, 10, 6993-7008, <https://doi.org/10.5194/acp-10-6993-2010>,
429 2010.
- 430 Sillman, S.: The relation between ozone, NOx and hydrocarbons in urban and polluted rural environments, *Atmospheric*
431 *Environment*, 33, 1821-1845, [https://doi.org/10.1016/S1352-2310\(98\)00345-8](https://doi.org/10.1016/S1352-2310(98)00345-8), 1999.
- 432 Sommariva, R., Cox, S., Martin, C., Borońska, K., Young, J., Jimack, P. K., Pilling, M. J., Matthaios, V. N., Nelson, B. S., and
433 Newland, M. J.: AtChem (version 1), an open-source box model for the Master Chemical Mechanism, *Geoscientific Model*
434 *Development*, 13, 169-183, <https://doi.org/10.5194/gmd-13-169-2020>, 2020.
- 435 Suris, F. N. A., Bakar, M. A. A., Ariff, N. M., Mohd Nadzir, M. S., and Ibrahim, K.: Malaysia PM₁₀ air quality time series
436 clustering based on dynamic time warping, *Atmosphere*, 13, 503, <https://doi.org/10.3390/atmos13040503>, 2022.
- 437 Tan, Y. and Wang, T.: What caused ozone pollution during the 2022 Shanghai lockdown? Insights from ground and satellite
438 observations, *Atmospheric Chemistry and Physics*, 22, 14455-14466, <https://doi.org/10.5194/acp-22-14455-2022>, 2022.
- 439 Tan, Z., Fuchs, H., Lu, K., Hofzumahaus, A., Bohn, B., Broch, S., Dong, H., Gomm, S., Häsel, R., and He, L.: Radical
440 chemistry at a rural site (Wangdu) in the North China Plain: observation and model calculations of OH, HO₂ and RO₂ radicals,
441 *Atmospheric Chemistry and Physics*, 17, 663-690, <https://doi.org/10.5194/acp-17-663-2017>, 2017.
- 442 Tan, Z., Lu, K., Hofzumahaus, A., Fuchs, H., Bohn, B., Holland, F., Liu, Y., Rohrer, F., Shao, M., and Sun, K.: Experimental
443 budgets of OH, HO₂, and RO₂ radicals and implications for ozone formation in the Pearl River Delta in China 2014, *Atmospheric*
444 *chemistry and physics*, 19, 7129-7150, <https://doi.org/10.5194/acp-19-7129-2019>, 2019.
- 445 Tian, J., Wang, Q., Zhang, Y., Yan, M., Liu, H., Zhang, N., Ran, W., and Cao, J.: Impacts of primary emissions and secondary
446 aerosol formation on air pollution in an urban area of China during the COVID-19 lockdown, *Environment International*, 150,
447 106426, <https://doi.org/10.1016/j.envint.2021.106426>, 2021.
- 448 Volkamer, R., Sheehy, P., Molina, L. T., and Molina, M. J.: Oxidative capacity of the Mexico City atmosphere-Part 1: A radical
449 source perspective, *Atmospheric Chemistry and Physics*, 10, 6969-6991, <https://doi.org/10.5194/acp-10-6969-2010>, 2010.
- 450 Wang, N., Xu, J., Pei, C., Tang, R., Zhou, D., Chen, Y., Li, M., Deng, X., Deng, T., and Huang, X.: Air quality during COVID-
451 19 lockdown in the Yangtze River Delta and the Pearl River Delta: Two different responsive mechanisms to emission reductions
452 in China, *Environmental Science & Technology*, 55, 5721-5730, <https://doi.org/10.1021/acs.est.0c08383>, 2021.
- 453 Wang, T., Xue, L., Brimblecombe, P., Lam, Y. F., Li, L., and Zhang, L.: Ozone pollution in China: A review of concentrations,
454 meteorological influences, chemical precursors, and effects, *Science of the Total Environment*, 575, 1582-1596,
455 <https://doi.org/10.1016/j.scitotenv.2016.10.081>, 2017.
- 456 Xue, L., Gu, R., Wang, T., Wang, X., Saunders, S., Blake, D., Louie, P. K., Luk, C. W., Simpson, I., and Xu, Z.: Oxidative
457 capacity and radical chemistry in the polluted atmosphere of Hong Kong and Pearl River Delta region: analysis of a severe
458 photochemical smog episode, *Atmospheric Chemistry and Physics*, 16, 9891-9903, <https://doi.org/10.5194/acp-16-9891-2016>,
459 2016.
- 460 Xue, R., Wang, S., Zhang, S., Zhan, J., Zhu, J., Gu, C., and Zhou, B.: Ozone Pollution of Megacity Shanghai during City-Wide
461 Lockdown Assessed Using TROPOMI Observations of NO₂ and HCHO, *Remote Sensing*, 14, 6344,
462 <https://doi.org/10.3390/rs14246344>, 2022.
- 463 Yang, X., Lu, K., Ma, X., Gao, Y., Tan, Z., Wang, H., Chen, X., Li, X., Huang, X., and He, L.: Radical chemistry in the Pearl
464 River Delta: observations and modeling of OH and HO₂ radicals in Shenzhen in 2018, *Atmospheric Chemistry and Physics*, 22,
465 12525-12542, <https://doi.org/10.5194/acp-22-12525-2022>, 2022.
- 466 Yang, X., Lu, K., Ma, X., Liu, Y., Wang, H., Hu, R., Li, X., Lou, S., Chen, S., and Dong, H.: Observations and modeling of OH
467 and HO₂ radicals in Chengdu, China in summer 2019, *Science of The Total Environment*, 772, 144829,
468 <https://doi.org/10.1016/j.scitotenv.2020.144829>, 2021.
- 469 Zhang, G., Hu, R., Xie, P., Lou, S., Wang, F., Wang, Y., Qin, M., Li, X., Liu, X., and Wang, Y.: Observation and simulation of
470 HOx radicals in an urban area in Shanghai, China, *Science of The Total Environment*, 810, 152275,
471 <https://doi.org/10.1016/j.scitotenv.2021.152275>, 2022a.
- 472 Zhang, K., Huang, L., Li, Q., Huo, J., Duan, Y., Wang, Y., Yaluk, E., Wang, Y., Fu, Q., and Li, L.: Explicit modeling of
473 isoprene chemical processing in polluted air masses in suburban areas of the Yangtze River Delta region: radical cycling and
474 formation of ozone and formaldehyde, *Atmospheric Chemistry and Physics*, 21, 5905-5917, <https://doi.org/10.5194/acp-21-5905-2021>, 2021.
- 475



476 Zhang, K., Liu, Z., Zhang, X., Li, Q., Jensen, A., Tan, W., Huang, L., Wang, Y., de Gouw, J., and Li, L.: Insights into the
477 significant increase in ozone during COVID-19 in a typical urban city of China, *Atmospheric Chemistry and Physics*, 22, 4853-
478 4866, <https://doi.org/10.5194/acp-22-4853-2022>, 2022b.
479 Zhu, J.: Why Did Ozone Concentrations Increase During Shanghai's Static Management? A Statistical and Radical Chemistry
480 Perspective (V1), Mendeley Data [dataset], 10.17632/3kmhg7r2df.1, 2023.
481 Zhu, J., Wang, S., Zhang, S., Xue, R., Gu, C., and Zhou, B.: Changes of NO₃ Radical and its Nocturnal Chemistry in Shanghai
482 from 2014 to 2021 Revealed by Long - term observation and a Stacking Model: Impact of China's Clean Air Action Plan,
483 *Journal of Geophysical Research: Atmospheres*, e2022JD037438, <https://doi.org/10.1029/2022JD037438>, 2022.
484 Zhu, J., Wang, S., Wang, H., Jing, S., Lou, S., Saiz-Lopez, A., and Zhou, B.: Observationally constrained modeling of
485 atmospheric oxidation capacity and photochemical reactivity in Shanghai, China, *Atmospheric Chemistry and Physics*, 20, 1217-
486 1232, <https://doi.org/10.5194/acp-20-1217-2020>, 2020.
487